machines

MDPI

Article

Numerical Analysis of The Temperature Characteristics of a Coal—Supercritical Water-Fluidized Bed Reactor for Hydrogen Production

Shiqi Wang, Rong Xie *, Jiali Liu, Pu Zhao, Haitao Liu and Xiaofang Wang

Key Laboratory of Ocean Energy Utilization and Energy Conservation, Ministry of Education, Dalian University of Technology, Dalian 116024, China; wangshiqi19971012@mail.dlut.edu.cn (S.W.)
* Correspondence: xieronz@dlut.edu.cn

Abstract: Supercritical water gasification (SCWG) of coal is a promising clean coal technology, which discards the traditional coal combustion and oxidation reaction to release carbon dioxide and other pollutants and replaces coal with a gasification reduction reaction in supercritical water to finally convert coal into a hydrogen-rich gas product with no net carbon dioxide emissions and no pollutant emissions, and thus has received much attention in recent years. However, the experimental conditions of coal to the hydrogen reactor are harsh, costly, and not easy to visualize and analyze, so numerical calculation and simulation analysis are important for the design, optimization, and industrial scaling-up of the reactor. In order to study the effect of the temperature field on the hydrogen production rate of the coal supercritical water gasification hydrogen production reactor, a numerical simulation calculation model is developed for this reactor in this paper. Comparing the experimental data in the literature, the maximum relative error of the gasification product yield per kg of coal between the two is less than 5%, which verifies the accuracy of the model built and the numerical method adopted in this paper. On this basis, the effects of supercritical water temperature and coal slurry temperature on the reactor's gasification products and reaction rate were investigated in depth. The results show that increasing the supercritical water temperature is beneficial to improve the reactor hydrogen production efficiency, while the high coal slurry temperature is not conducive to adequate reaction, thus reducing the hydrogen production efficiency. For the laboratory coal supercritical water gasification to hydrogen reactor studied in this paper, the ideal temperature of supercritical water is 850~900 K, and the ideal temperature of coal slurry is 400–450 K. The conclusions of this paper can provide some reference for subsequent industrial scale-up studies of the reactor.

Keywords: supercritical water gasification; hydrogen production reactor; numerical simulation; temperature characteristics; hydrogen production rate

Citation: Wang, S.; Xie, R.; Liu, J.; Zhao, P.; Liu, H.; Wang, X. Numerical Analysis of The Temperature Characteristics of a Coal—Supercritical Water-Fluidized Bed Reactor for Hydrogen Production. *Machines* **2023**, *11*, 546. https://doi.org/10.3390/machines11050546

Academic Editors: Imre Ferenc Barna and Krisztian Hriczo

Received: 3 April 2023
Revised: 29 April 2023
Accepted: 8 May 2023
Published: 12 May 2023

1. Introduction

China has proposed the goal of achieving carbon peaking by 2030 and carbon neutrality by 2060 [1]. To reach this goal, the supporting role of science and technology innovation should be given full play to promote the continuous optimization of China's energy structure, facilitate the reduction of carbon emission intensity, and promote industrial restructuring [2]. However, there are still some shortcomings in the utilization efficiency of new energy technologies, the promotion and application of green low-carbon technologies, and even the systematic capacity building of related technological innovation in China [3,4]. As the country with the world's largest coal reserves, how to use coal resources reasonably and cleanly has become an important issue.

Supercritical water gasification (SCWG) is a promising clean coal technology that converts coal into a hydrogen-rich gas product with no CO2 release and no pollutant emissions and therefore has received a lot of attention in recent decades [5–7]. Water has special physicochemical properties in the supercritical state, such as high diffusivity, low

viscosity, and good miscibility with various organic substances, which determine it to be a good chemical reaction medium [8–11]. At present, numerical calculations have become an important tool for studying SCWG technology because of the strict conditions required for the reaction and the high experimental cost due to high temperature and pressure. Ren et al. developed a three-dimensional transient CFD model of a supercritical water-fluidized bed hydrogen production reactor for coal based on the Euler–Lagrange method with coupled chemical reaction kinetics model [12]. Ou et al. provided heat for SCWG of the coal in an integrated supercritical water reactor (ISWR) combined with subsequent product oxidation, which offers an effective method for directional control of the temperature field [13]. Guo, Jin, and Zhang established the reaction kinetics, improved the reactor model, and advanced the simulation modeling work [14–17].

Zhao et al. used a Gaussian process surrogate model with effective adaptive sampling to develop a stable numerical simulation model for the SCWFB reactor for subsequent analysis [18]. Particles within fluidized beds face a high degree of complexity. And Maryamd et al. thoroughly investigated these complexities by studying particle–particle, particle–droplet, and particle–liquid interactions in order to understand the process [19] better.

In terms of strengthening the supercritical water coal gasification process, Lv et al. revealed that the controlled step of the supercritical water coal gasification process lies in the ring-opening reaction of thick ring aromatics. The model of porous coke particle gasification in supercritical water was established, and its gasification mechanism and influence rules were obtained [20].

The transformation of coal particle packets in supercritical water (SCW) was studied by Vostrikov et al. Experimental results were analyzed in the framework of homogeneous, non-reactive core and stochastic pore models. The quantitative composition of the transformation products was determined. The dependence of the conversion rate on the degree of coal conversion, reaction time, and temperature was described under the assumptions of first-order reactions and Arrhenius dependence [21].

Zhang et al. completed a wall-bed heat transfer model in SCWFB with an appropriate selection of physical properties of the bales and tested seven thermal conductivity models for the mixture. A simplified spherical particle model was used to describe the thermal resistance between the wall and the packet. Then, the heat transfer coefficients of the models based on the packet renewal theory were compared with those of the empirical correlation method [22].

Yao et al. numerically investigated the physical field, residence time, and gas yield of the SCWFB reactor based on the Eulerian two-fluid approach and particle flow kinetic theory. In addition, the effects of operating conditions and reactor structure on gas yield and residence time were investigated to explore the best operating rules to increase gas yield. The results of this work may be of interest to operators trying to obtain more information about the reactor and guide the design of SCWFB reactors [23].

The temperature characteristics are a key factor affecting the reactor efficiency. However, previous investigations on the temperature characteristics in the reactor are not sufficient. To deeply study the temperature characteristics of an SCWFB reactor, in this paper, a three-dimensional transient model is numerically simulated based on the chemical reaction dynamics model coupled with the radiation model. The computational results fit well with the experimental values. Based on this model, this paper then explores the effects of supercritical water temperature and coal slurry temperature on the reactor product yield, internal reaction rate, and other factors and proposes reaction conditions in favor of supercritical water reactor efficiency improvement. The conclusions obtained in this paper can provide a reference for the following reactor optimization design.

2. Numerical Model

2.1. Physical Model

In this section, a three-dimensional computational model of multiphase flow and chemical reaction kinetics with an internal heating device will be developed to simulate the

process of gasification participating in the reaction inside a supercritical water gasification reactor. The physical model is shown in Figure 1a. The total height of the reactor is 1750 mm, the inner diameter is 60 mm, and the outer diameter is 120 mm [12]. The coal slurry flows into the reactor from the inlet on the side wall of the reactor. And the supercritical water flows into the reactor from the bottom of the reactor and the reaction occurs after mixing. The reactor is equipped with heating rods at the bottom. The diameter of the single heating rod is 10 mm, and the height is 900 mm. The total heating power of the heating rods is 2000 w. g is the constant of gravity. g has a constant value of 9.81 m/s^2. The grid is partially encrypted with a hexahedral grid, and the total number of grids is 667,194, as Figure 1b.

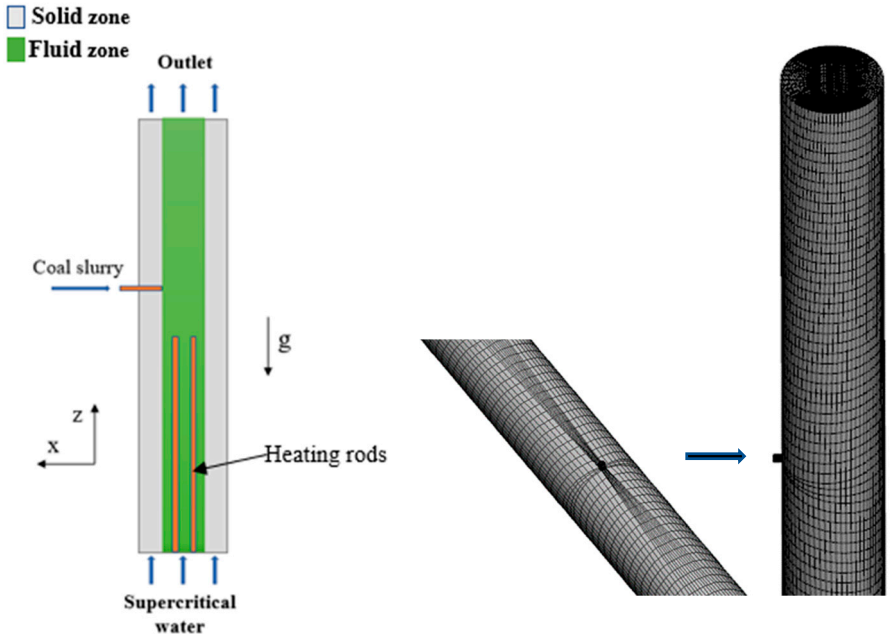

Figure 1. Schematic diagram of fluidized bed (**a**) as well as (**b**) Partial grids.

The operating pressure of the whole reactor is maintained at 23 MPa. Supercritical water enters through the inlet at the bottom of the reactor, while coal slurry enters through the inlet at the side wall. As the slurry enters and is heated in the reactor, the coal particles decompose and react to produce gaseous products such as H_2, CO, CO_2, CH_4, etc., which escape from the top of the reactor. The high temperature in the reactor is mainly heated by the wall thermostat and the heating rods in the lower part of the reactor.

2.2. Governing Equations

Continuous phase equation within the multiphase flow model:

$$\frac{\partial}{\partial t}(\alpha_l \rho_l) + \nabla(\alpha_l \rho_l \vec{v}_l) = C_m \tag{1}$$

where the subscript l represents the fluid-related parameter, α_l represents the volume fraction, and C_m represents the material transfer between the two phases.

The conservation of momentum equation:

$$\begin{aligned} &\tfrac{\partial}{\partial t}(\alpha_l \rho_l \vec{v}_l) + \nabla(\alpha_l \rho_l \vec{v}_l \vec{v}_l) = -\alpha_l \nabla p + \nabla(\partial_l \overline{\overline{\tau_l}}) \\ &+\partial_l \rho_l \vec{g} + K_{ls}(\vec{v}_s - \vec{v}_l) + C_m \vec{v_{ls}} \end{aligned} \tag{2}$$

where $\vec{g}$ is the constant vector, $\overline{\overline{\tau_l}}$ is the viscous stress tensor, $\vec{v_{ls}}$ is the interphase velocity, and K_{ls} is the two phases' momentum exchange coefficient.

In this paper, the Gidaspow drag model is used to calculate the drag force between the two phases, defined by the following equation:

$$K_{ls} = \frac{3}{4} C_D \frac{\alpha_s \alpha_l \rho_l \left| \vec{v_s} - \vec{v_l} \right|}{d_s} \alpha_l^{-2.65} \ (\alpha_l \ > \ 0.8) \tag{3}$$

$$K_{ls} = 150 \frac{\alpha_s^2 \mu_l}{\alpha_l d_s^2} + 1.75 \frac{\alpha_s \rho_l \left| \vec{v_s} - \vec{v_l} \right|}{d_s} \ (\alpha_l \ \leq \ 0.8) \tag{4}$$

where the term with subscript s represents the solid phase, α_s is the volume fraction of the solid phase, d_s is the coal particle diameter, C_D is the interphase drag coefficient, and the specific expression is:

$$C_D = \frac{24}{\alpha_l \mathrm{Re}_s} \left[1 + 0.15 (\alpha_l \mathrm{Re}_s)^{0.687} \right] \tag{5}$$

where Re_s is the Reynolds number of solid phase, the specific expression is:

$$\mathrm{Re}_s = \frac{\rho_l d_s \left| \vec{v_s} - \vec{v_l} \right|}{\mu_l} \tag{6}$$

The specific expression for the equation of energy conservation in the reactor is:

$$\begin{array}{c} \frac{\partial}{\partial t} (\alpha_l \rho_l h_l) + \nabla \cdot (\alpha_l \rho_l \vec{v_l} h_l) = \alpha_l \frac{ds}{dt} + Q_{sl} + \\ \nabla \cdot (\lambda \nabla T - \sum_i h_i J_i) + \overline{\overline{\tau_l}} : \nabla \vec{v_l} - \nabla \cdot q_r + H_{r,s} \end{array} \tag{7}$$

$h_l = \sum_j Y_j h_j$, λ is the thermal conductivity of the fluid term, Q_{sl} is the energy transfer term between the two phases, $\nabla \cdot q_r$ is the radiative heat transfer term, and $H_{r,s}$ is the enthalpy of production of each reaction in the fluid phase.

The specific expression for the radiative heat transfer equation in the reactor is:

$$\begin{array}{c} \frac{dI(\vec{r}, \vec{s})}{ds} = k_l \frac{\sigma T_l^4}{\pi} + Es - (k_l + k_s + \sigma_s) \cdot \\ I(\vec{r}, \vec{s}) + \frac{\sigma_s}{4\pi} \int_0^{4\pi} I(\vec{r}, \vec{s'}) \Phi(\vec{s}, \vec{s'}) d\Omega' \end{array} \tag{8}$$

$Es = \sum_i \varepsilon_s, in_i A_s, i \frac{\sigma T_{s,i}^4}{\pi}$ is the equivalent radiation energy of the solid term; $k_s = \sum_i \varepsilon_s, in_i A_s, i$ is the radiation absorption coefficient of the solid term; $\sigma_s = \sum_i (1 - f_{s,i})$ $(1 - \varepsilon_{s,i}) n_i A_{s,i}$, is the particle scattering coefficient of the solid term; where and are the emissivity $\varepsilon_{s,i}$ and $f_{s,i}$ scattering factor of the particle; k_l is the radiation absorption coefficient of the fluid phase.

The specific expression for the radiation term $\nabla \cdot q_r$ is as follows:

$$-\nabla \cdot q_r = (k_l + k_s) \int_o^{4\pi} I(\vec{r}, \vec{s}) d\Omega - 4\pi \cdot \left(k_l \frac{\sigma T_l^4}{\pi} + \sum_i \varepsilon_{s,i} n_i A_{s,i} \frac{\sigma T_{s,i}^4}{\pi} \right) \tag{9}$$

The specific expression of the component transport equation in the reactor is:

$$\frac{\partial}{\partial t} (\alpha_l \rho_l Y_{l,i}) + \nabla \cdot (\alpha_l \rho_l Y_{l,i} \vec{v_l}) = \nabla \cdot (\alpha_l \rho_l D_{i,m} \nabla Y_{l,i}) + S_i \tag{10}$$

$Y_{l,i}$ and $D_{i,m}$ are the mass fraction and the diffusion coefficient of each component in the fluid term, respectively, and are the source terms of the components for each reaction.

2.3. Reaction Kinetics

The reaction mechanism in the reactor is complex. The thermal decomposition of coal in supercritical water produces volatile carbon and solid-phase residual carbon. Volatile and solid carbon react with supercritical water to produce gasification products, and the mechanistic model of the coal supercritical water gasification reaction built in this paper refers to Reference [15] with the following specific chemical reactions:

(1) High-temperature hydrolysis reaction of volatile carbon

$$Vol \xrightarrow{K_1} H_2 \tag{11}$$

$$Vol \xrightarrow{K_2} \mathrm{CO} \tag{12}$$

$$Vol \xrightarrow{K_3} CH_4 \tag{13}$$

$$Vol \xrightarrow{K_4} CO_2 \tag{14}$$

(2) Steam reforming reaction of fixed carbon

$$C + H_2O \xrightarrow{K_5} H_2 + CO \tag{15}$$

$$C + 2H_2O \xrightarrow{K_6} 2H_2 + CO_2 \tag{16}$$

(3) Water–gas conversion reaction

$$CO + H_2O \xrightarrow{K_7} H_2 + CO_2 \tag{17}$$

(4) Methanation reaction

$$CO + 3H_2 \xrightarrow{K_8} CH_4 + H_2O \tag{18}$$

The above equation provides an overall consideration of the gasification reaction of coal in supercritical water. It considers all the potential gas-forming pathways and avoids the cumbersome description of intermediate product conversion. Each reaction can meet the primary reaction characteristics in the reactor, which is in accordance with Arrhenius' law. And the reaction rate constants and temperature relationships for each reaction are as follows:

$$k = Aexp\left(-\frac{E}{RT}\right) \tag{19}$$

A is the prefactor, E is the activation energy in kJ/mol, and R is the ideal gas constant.

2.4. Numerical Solution Method and Boundary Conditions

In the reactor, the fluid-particle dual-phase flow is simulated using the dense discrete phase model (DDPM) [24]. The Euler–Lagrange method is used to solve the continuous flow field, where the fluid is considered as a continuous body by solving the Navier–Stokes equation, while the discrete phase is solved by tracking a large number of particles in the computational flow field. Since supercritical water has good solubility for gaseous products, the fluid mixture can be considered a homogeneous phase, and the k-ε turbulence model is used to solve the flow of the fluid. The Gidaspow Resistance Law is used to calculate the resistance [25], and a discrete dimensional (D.O.) model is used to solve the radiation heat transfer problem within the reactor, which can solve the radiation problem from surface to surface. The particle emissivity used in this paper is set to 0.9. The coal particles are assumed to be spherical and follow the Rosin–Rammler diameter distribution function, the

slurry is at 30% concentration, and the slurry temperature is 298 K. The detailed physical parameters are shown in Tables 1 and 2.

Table 1. Coal particle properties.

Min. Diameter (mm)	Max. Diameter (mm)	Mean Diameter (mm)	Spread Parameter
0.075	0.3	0.2264	3.3185
Scattering Factor	**Emissivity**	**Density (kg/m^3)**	**Specific Heat (J/kg·K)**
0.6	0.9	1300	1680

Table 2. Analysis of the Yimin Coal.

Parameters	Yimin Coal (wt%)
Proximate analysis (air dried)	
Moisture	18.42
Fixed carbon	33.73
Volatile matter	32.21
Ash	15.46
Ultimate analysis (dry base)	
C	40.5
H	3.25
N	0.57
S	0.19
O	21.43

The pressure inside the reactor is maintained at 23 MPa, and the products or reactants, such as water under high temperature and pressure, will keep to the supercritical state. The physical properties change violently. In order to calculate accurately, the paper uses a combination of NIST and AP1700 database physical properties to attain accurate physical properties. The physical properties results are coupled into the simulation calculation model using the method of writing UDF. The characterization accuracy is significantly improved compared with the former, and the accuracy of the calculation results is also significantly improved. The absorption radiation coefficient of supercritical water is obtained by the LBL method and coupled with the Planck calculation method, and the physical properties of the mixture are calculated by taking the mass-weighted average of each component.

The ANSYS FLUENT 2022 R1 solver is used to solve the control equations of the SCWFB reactor. The Renormalization Group (RNG) $k-\varepsilon$ turbulence model is used for the continuous field solution. The control equations are discretized in first-order windward format, and the solver selects the Phase Coupled Simple method for solving, with the relaxation factor set in the range of 0.4~0.9, the time step set to 0.01 s, and the calculation time of 100 s. The SCWFB boundary conditions are set in Table 3.

Table 3. Boundary condition setting.

Boundary Conditions	
Coal slurry	Mass flow inlet
Supercritical water	Mass flow inlet
Outlet	Pressure outlet
Outer wall	Constant temperature wall
Interface	Coupled wall
Heating rod	Constant heat flux

3. Model Validation

3.1. Distribution of Components

Based on the model established in the previous section, the transient 100 s calculation was run for the reactor, and the transient results of the molar fraction distribution of the gasification products are shown in Figure 2, and the results of the temperature and flow fields are shown in Figure 3.

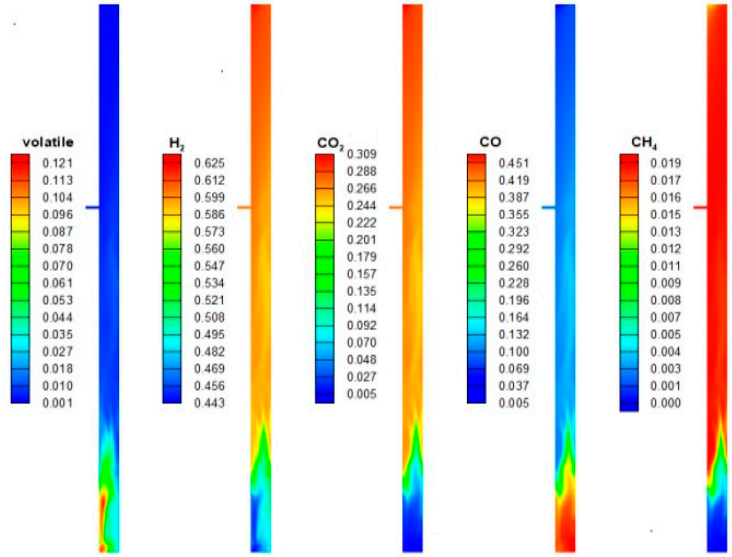

Figure 2. Distribution of gasification products.

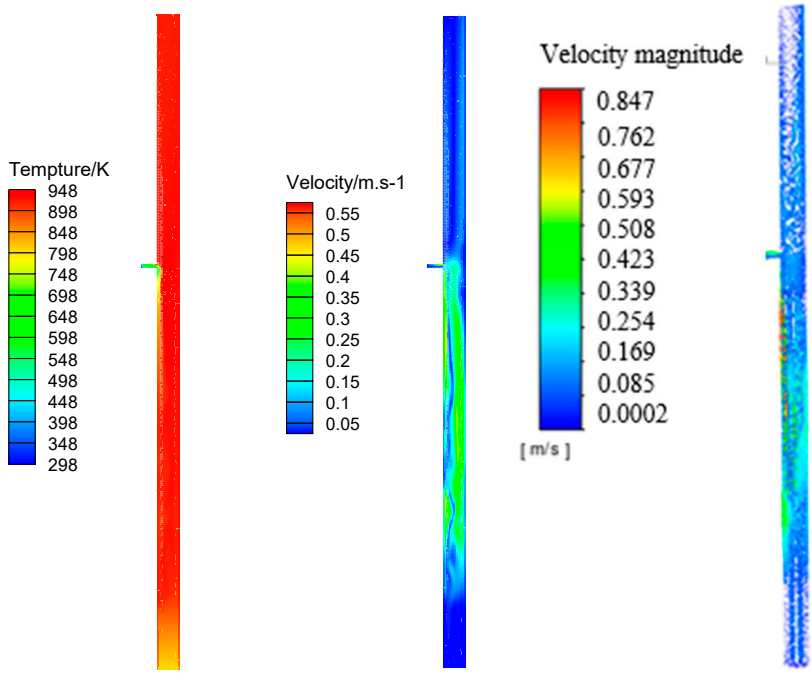

Figure 3. The temperature field and flow field.

According to the calculation results, it can be seen that the coal slurry enters the reactor and moves rapidly toward the bottom of the reactor under the influence of gravity, and continues to absorb heat during the descent, and the temperature gradually increases and gradually volatilizes to participate in the reaction, thus more gathered at the bottom of the reactor, which is consistent with the calculation results. The distribution form of other gasification products is related to the distribution of the reaction proceeding. The bottom

of the reactor is the main place where the volatile carbon high-temperature hydrolysis reaction is carried out due to the gathering of coal particles, while the water–gas conversion reaction is dominated in the middle and upper parts. Therefore, carbon monoxide is more distributed in the bottom of the reactor, while hydrogen, carbon dioxide, and methane are mainly distributed in the middle and upper parts of the reactor. The overall distribution pattern and the molar fraction share are similar to those of Reference [12].

The temperature field of the reactor is relatively stable due to the wall temperature, and the temperature at the slurry inlet and supercritical water inlet decreases, which is consistent with the actual situation. The flow velocity of the overall flow field of the reactor is low, and at the slurry inlet, the slurry moves downward while the supercritical water moves upward, and the strong convection between the two forms helps to mix fully, which is conducive to the full reaction.

3.2. Simulated and Experimental Values

While for CFD, the accuracy of the model calculation is the key to ensuring that the subsequent study is meaningful. To verify the accuracy of the model, the calculated results were compared with the experimental results within Reference [12], and the comparison of the yield results is shown in Figure 4. The detailed operating conditions of the simulations are given in Table 4.

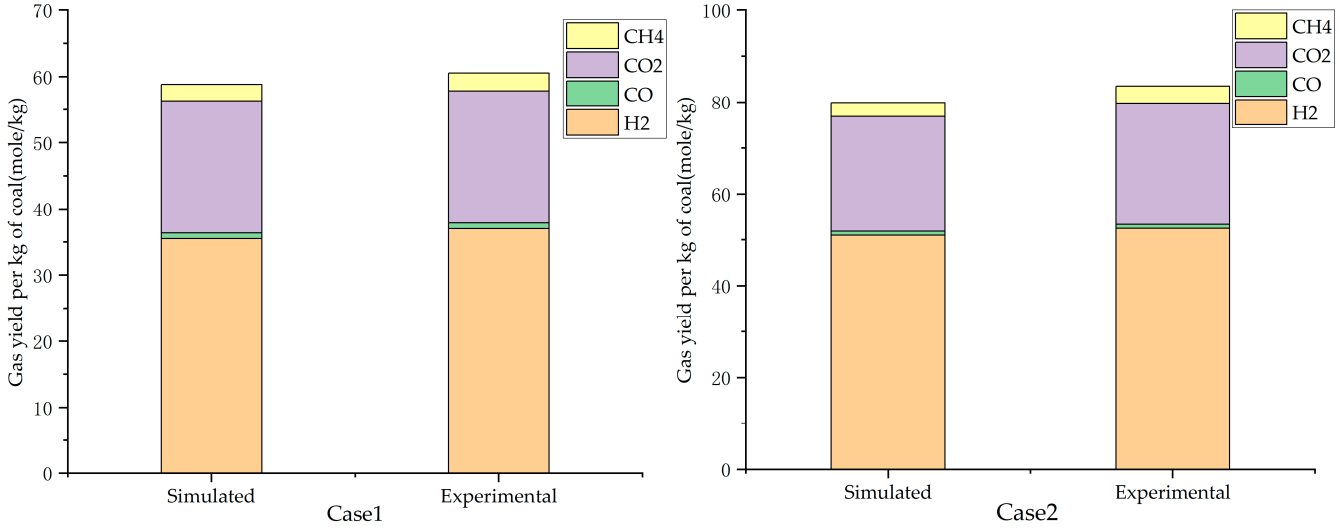

Figure 4. Comparison of simulated and experimental gas yields.

Table 4. Operating conditions of the SCWFB reactor.

Operating Conditions	Case1	Case2
Mass flow rate of the coal slurry (g/s)	0.3	0.3
Temperature of coal slurry (K)	298	298
Coal slurry concentration (wt%)	30	30
Mass flow rate of SCW (g/s)	2.7	2.7
Temperature of SCW (K)	773	823
Temperature of outer wall (K)	923	923
Total power of heating roads (w)	2000	2000

After comparing the model calculation results with the experimental values, the relative error value is less than 5%. The simulation results are in good agreement with the experimental results, and the calculation accuracy of the model is good, which can be used as a basis for further investigation of other characteristics within the reactor.

4. Temperature Characteristics

4.1. Effect of Supercritical Water Temperature on Yield and Reaction Rate

The content of supercritical water, the most abundant substance inside the reactor, is close to 90% mole fraction. Various reactants and intermediates in the reactor are infiltrated into the supercritical water environment for various reactions. Hence, the temperature of supercritical water significantly impacts the value of the internal reactor temperature field and the distribution of each reaction and product in the reactor. Therefore, it is necessary to investigate the effect of supercritical water temperature on the yield of gasification products and each reaction in the reactor. In this paper, the steady-state results of the reactor were calculated for the temperature range of supercritical water from 673 K to 1073 K. In the meantime, the wall temperature, slurry temperature, and slurry mass flow rate are kept constant. The wide temperature range includes the starting temperature required for the reaction and the ultra-high temperature beyond the wall temperature, which can fully reveal the influence of supercritical water temperature on the reactor. The variation curves of each gasification product with the temperature of supercritical water are shown in Figure 5.

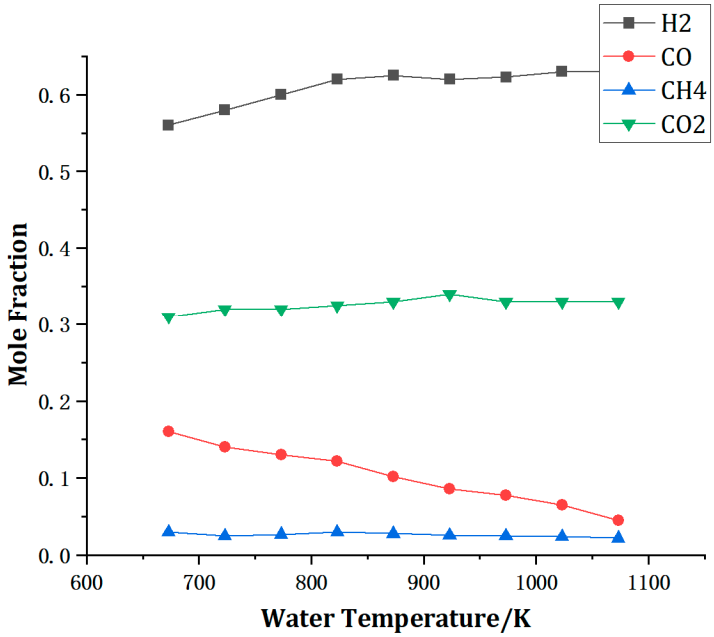

Figure 5. Mole fraction of gasification products.

The mole fraction of hydrogen increased with the supercritical water temperature from 673 K to 873 K. The mole fraction of hydrogen remained relatively stable during the variation of the supercritical water temperature from 873 K to 1073 K. The trend of carbon dioxide is similar to hydrogen, and the mole fraction of carbon dioxide reaches the maximum when the supercritical water temperature reaches 923 K. The effect of continuing to increase the supercritical water temperature on the mole fraction of carbon dioxide is low. The trend of carbon monoxide is opposite to that of hydrogen and carbon dioxide, and the mole fraction of carbon monoxide gradually decreases during the change of supercritical water temperature from 673 K to 1073 K. The trend of the overall change of methane was smooth, and the molar fraction of methane did not show significant fluctuations throughout the temperature change interval of supercritical water. The yield change of the product is essentially a change in the reaction rate. Comparing the rates of the reactions in the reactor and verifying the calculations, the rate change curve of each chemical reaction is shown in Figure 6a–d.

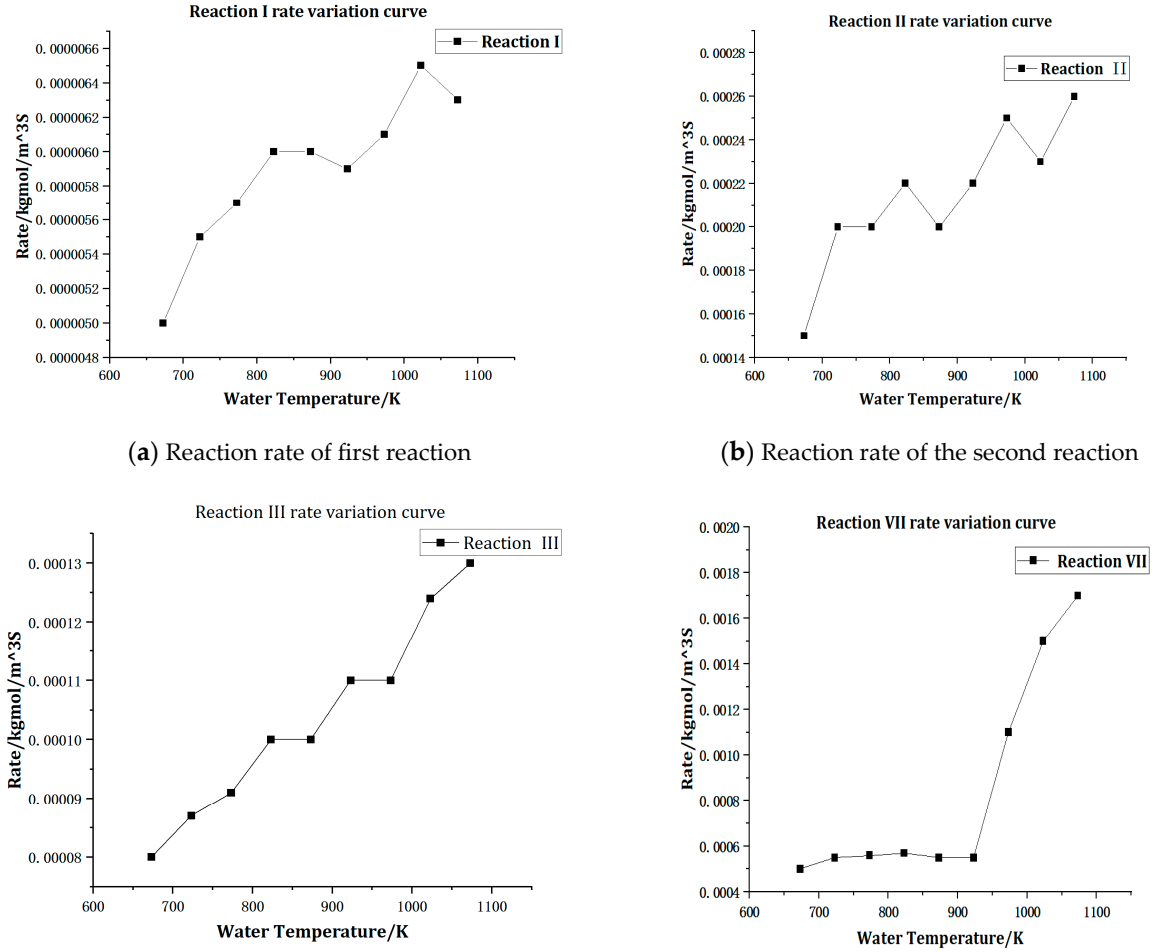

(**a**) Reaction rate of first reaction

(**b**) Reaction rate of the second reaction

(**c**) Reaction rate of third reaction

(**d**) Reaction rate of seventh reaction

Figure 6. The reaction rate of the critical reactions.

As can be shown above, with the increase in the supercritical water temperature, the trend of each chemical reaction rate is similar to that of the wall temperature increase, with some fluctuations. The reaction rate of reaction VII increased rapidly after the supercritical water temperature exceeded 923 K. This is because when the supercritical water temperature exceeded the wall temperature, the warming effect of supercritical water on the reactor as a whole was significantly enhanced, and the overall temperature increase in the reactor increased, and each reactant was immersed in the high-temperature supercritical water reaction VII as the main reaction affecting the reactor products was decisive for the influence of each product.

The conversion of the mass and energy content of the raw material into a gaseous product is important. Thus, carbon conversion efficiency, defined as the ratio of carbon in the gaseous product to total carbon in the feedstock, is used to quantify the conversion of the SCWFB reactor.

The CE criterion is expressed mathematically as:

$$CE(\%) = \frac{n_{CO_2} + n_{CO} + n_{CH_4}}{n_{c,feedstock}} \times 100\% \quad (20)$$

where n_{CO_2}, n_{CO}, n_{CH_4}, and $n_{c,feedstock}$ represent the carbon moles in CO_2, CO, CH_4, and the feedstock, respectively. The variation curve of CE is shown in Figure 7.

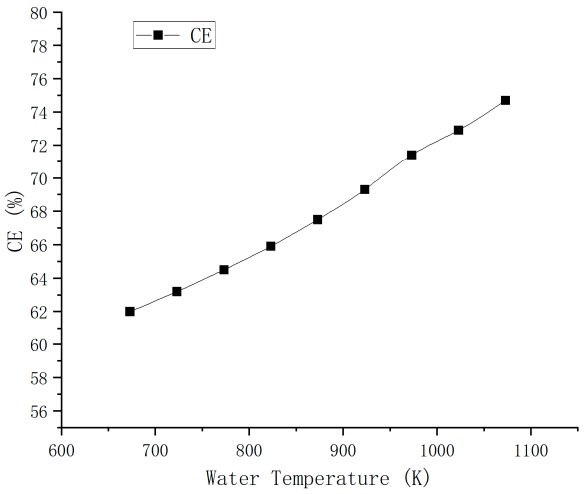

Figure 7. Effect of scw temperature.

With the increase in the supercritical water temperature, the CE also increases gradually. It means that the reaction inside the reactor also goes on more completely, which is beneficial for the operation of the reactor.

4.2. Effect of Coal Slurry Temperature on the Reactor

The coal slurry carries coal particles into the reactor, which has little effect on the overall temperature of the reactor due to the small flow rate but has a significant effect on the gasification rate and efficiency of the coal particles, which directly affects the efficiency and yield of the reactor. To validate the analysis and assumptions, in this paper, the variation curves of gasification products were calculated for coal slurry temperatures from 398 K to 698 K with a temperature interval of 100 K, as shown in Figure 8. The mole fraction of hydrogen and carbon dioxide decreases as the slurry temperature increases, while the mole fraction of carbon monoxide increases, and methane remains relatively stable. This is in contrast to the effect of the increase in supercritical water temperature on the reactor obtained in the previous calculations.

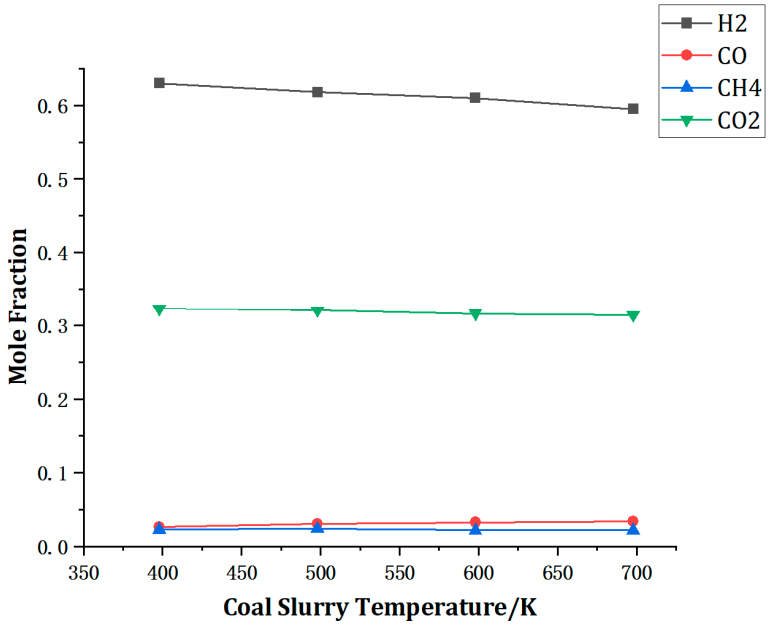

Figure 8. Mole fraction of gasification products.

The average particle diameter was calculated by selecting the cross-section of 600 mm height under the slurry inlet; it was found that the average particle diameter decreased gradually with the increase in slurry temperature, and the change curve of coal particle diameter and the comparison graphs at 398 K and 698 K were shown in Figures 9 and 10a,b. Due to the increase in coal slurry temperature, the decomposition rate of coal particles accelerates, and they are rapidly converted into volatile carbon. Under the rapid blowing of the lower supercritical water, the distribution of volatile carbon keeps moving upward, which leads to the escape from the reactor without sufficiently reacting with supercritical water for high-temperature hydrolysis, which affects the sufficient reaction of the reactor and is not conducive to the efficient operation of the reactor. Therefore, in order to improve the operating efficiency of the reactor, the inlet temperature of the slurry should be kept at 398 K. A lower slurry temperature requires a longer heating time for the coal particles to reach the required temperature for hydrolysis, which will increase the cost of the reaction and also reduce the reaction efficiency of the reactor in disguise, so the slurry temperature should not be used too low.

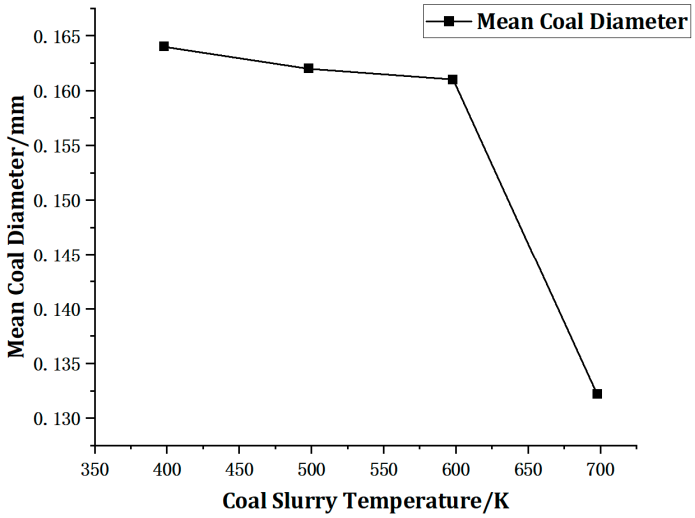

Figure 9. Mean particle diameter.

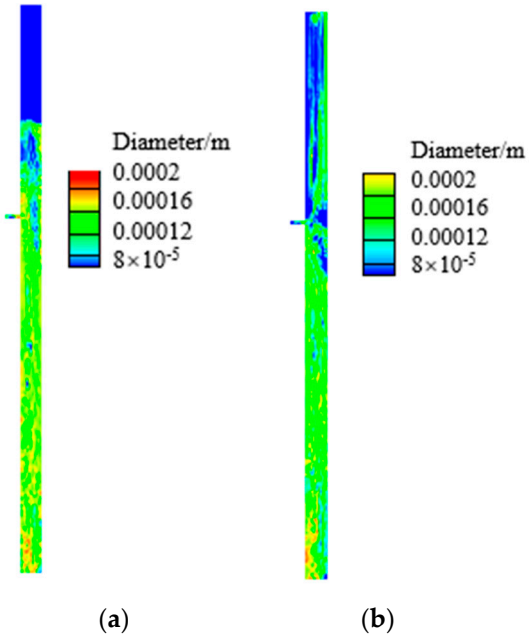

Figure 10. The 398 K particle diameter (**a**), as well as the 698 K particle diameter (**b**).

5. Conclusions

This paper establishes a complete three-dimensional model for the supercritical water coal gasification hydrogen reactor. A three-dimensional transient CFD model is built based on the existing simplified chemical reaction model. The error is within 5% after comparing it with the experimental data, which verifies the accuracy and efficiency of the numerical calculation model in this paper. Since the experimental conditions of coal to hydrogen reactor are costly and not easy to visualize and analyze, the numerical calculation and simulation analysis is of great significance for the reactor's design, optimization, and industrial scaling-up. Based on this, the following specific conclusions are drawn by investigating the relevant factors affecting the internal temperature field of the reactor:

After comparing the content of gasification products at a wide range of supercritical water temperature and coal slurry temperature, it can be found that water temperature and coal slurry temperature have opposite effects on the reactor gasification products.

As the reactions in the reactor are heat absorption reactions, the increase in supercritical water temperature can accelerate the reflection, and the hydrogen production rate is the largest when the supercritical water temperature is 850~900 K. The increase in slurry inlet temperature will accelerate the decomposition rate of coal particles. Too rapid decomposition is not conducive to fully mixing coal particles and supercritical water, reducing the time particles stay in the reactor and the reaction efficiency. The slurry temperature control at 400~450 K is conducive to the full reaction.

Author Contributions: Conceptualization, S.W., R.X. and J.L.; methodology, S.W., R.X., J.L. and H.L.; software, S.W., J.L. and P.Z.; validation, S.W., J.L. and P.Z.; formal analysis, S.W.; investigation, S.W.; investigation, S.W., R.X. and J.L.; data curation, S.W.; writing—original draft preparation, S.W.; writing—review and editing, S.W.; visualization, S.W.; supervision, R.X., H.L. and X.W.; project administration, R.X. and X.W.; and funding acquisition, R.X., X.W. and H.L. All authors have read and agreed to the published version of the manuscript.

Funding: This work was supported by the National Key Research and Development Program of China (2020YFA0714403).

Data Availability Statement: Not applicable.

Conflicts of Interest: The authors declare no conflict of interest.

Abbreviations

The following abbreviations are used in this manuscript:

SCWG	Supercritical water gasification
CFD	Computational fluid dynamics
SCWB	Supercritical water-fluidized bed
UDF	User designed function
ISWR	Integrated supercritical water reactor
LBL	Line by line
D.O.	Discrete ordinate
DDPM	Dense discrete phase model
SCW	Supercritical water
VOL	Volatile carbon

References

1. Shi, Z.; Shi, X. Efforts to Promote the Achievement of Carbon Neutrality. *Red Flag Manuscr.* **2021**, 4.
2. Liu, R.H.; Wang, G.; Huang, N.; Ding, M.L. Research on the path of China's science and technology innovation to support carbon peaking and carbon neutrality. *Guangxi Soc. Sci.* **2021**, *8*, 1–7.
3. Xu, J.; Rao, L. Analysis of the current situation and prospect of hydrogen energy application. *Stand. Qual. Mach. Ind.* **2021**, *4*, 39–42.
4. Xu, S.; Yu, B. Current status and future prospects of hydrogen energy technology development in China. *J. Beijing Univ. Technol.* **2021**, *23*, 1–12.

5. Jin, H.; Fan, C.; Guo, L.; Liu, S.; Cao, C.; Wang, R. Experimental study on hydrogen production by lignite gasification in supercritical water fluidized bed reactor using external recycle of liquid residual. *Energy Convers. Manag.* **2017**, *145*, 214–219. [CrossRef]
6. Lan, R.; Jin, H.; Guo, L.; Ge, Z.; Guo, S.; Zhang, X. Hydrogen Production by Catalytic Gasification of Coal in Supercritical Water. *Energy Fuels* **2014**, *28*, 6911–6917. [CrossRef]
7. Fan, C.; Guo, S.; Jin, H. Numerical study on coal gasification in supercritical water fluidized bed and exploration of complete gasification under mild temperature conditions. *Chem. Eng. Sci.* **2019**, *206*, 134–145. [CrossRef]
8. Guo, L.; Jin, H. Boiling coal in water: Hydrogen production and power generation system with zero net CO2 emission based on coal and supercritical water gasification. *Int. J. Hydrogen Energy* **2013**, *38*, 12953–12967. [CrossRef]
9. Wang, R.; Guo, L.; Jin, H.; Lu, L.; Yi, L.; Zhang, D.; Chen, J. DFT study of the enhancement on hydrogen production by alkaline catalyzed water gas shift reaction in supercritical water. *Int. J. Hydrogen Energy* **2018**, *43*, 13879–13886. [CrossRef]
10. Jin, H.; Zhao, X.; Guo, L.; Zhu, C.; Cao, C.; Wu, Z. Experimental investigation on methanation reaction based on coal gasification in supercritical water. *Int. J. Hydrogen Energy* **2017**, *42*, 4636–4641. [CrossRef]
11. Jin, H.; Wang, C.; Fan, C.; Guo, L.; Cao, C.; Cao, W. Experimental investigation on the influence of the pyrolysis operating parameters upon the char reaction activity in supercritical water gasification. *Int. J. Hydrogen Energy* **2018**, *43*, 13887–13895. [CrossRef]
12. Ren, Z.; Jin, F.; Liu, S.; Ou, Z. Numerical analysis of particle flow and heat transfer characteristics in a supercritical water fluidized bed hydrogen production reactor for coal. *J. Eng. Thermophys.* **2020**, *41*, 154–160.
13. Ou, Z.; Jin, H.; Ren, Z.; Zhu, S.; Song, M.; Guo, L. Mathematical model for coal conversion in supercritical water: Reacting multiphase flow with conjugate heat transfer. *Int. J. Hydrogen Energy* **2019**, *44*, 15746–15757. [CrossRef]
14. Ge, Z.; Guo, L.; Jin, H. Hydrogen production by non-catalytic partial oxidation of coal in supercritical water: The study on reaction kinetics. *Int. J. Hydrogen Energy* **2017**, *42*, 9660–9666. [CrossRef]
15. Liu, S.; Guo, L.; Jin, H.; Li, L. Hydrogen production by supercritical water gasification of coal: A reaction kinetic model including nitrogen and sulfur elements. *Int. J. Hydrogen Energy* **2020**, *45*, 31732–31744. [CrossRef]
16. Su, X.; Guo, L.; Jin, H. Mathematical Modeling for Coal Gasification Kinetics in Supercritical Water. *Energy Fuels* **2016**, *30*, 9028–9035. [CrossRef]
17. Zhang, H.; Lv, Y.J. Numerical simulation of two-phase flow characteristics of supercritical water circulating fluidized bed. *J. Eng. Thermophys.* **2018**, *39*, 127–132.
18. Zhao, P.; Liu, H.; Xie, X.; Wang, S.; Liu, J.; Wang, X.; Xie, R.; Zuo, S. Efficient Surrogate-Assisted Parameter Analysis for Coal-Supercritical Water Fluidized Bed Reactor with Adaptive Sampling. *Machines* **2023**, *11*, 295. [CrossRef]
19. Askarishahi, M.; Salehi, M.-S.; Radl, S. Challenges in the Simulation of Drying in Fluid Bed Granulation. *Processes* **2023**, *11*, 569. [CrossRef]
20. Lv, Y.; Jin, H.; Li, G.; Wang, H. Research progress on coal utilization technology based on supercritical water gasification for hydrogen production. *J. Coal* **2022**, *47*, 3870–3885. [CrossRef]
21. Vostrikov, A.A.; Psarov, S.A.; Dubov, D.Y.; Fedyaeva, O.N.; Sokol, M.Y. Kinetics of Coal Conversion in Supercritical Water. *Energy Fuels* **2007**, *21*, 2840–2845. [CrossRef]
22. Zhang, T.; Lu, Y. Modeling of Wall-to-Bed Heat Transfer in a Supercritical Water Fluidized Bed by the Packet Approach. *Ind. Eng. Chem. Res.* **2020**, *59*, 22640–22655. [CrossRef]
23. Yao, L.; Lu, Y. Supercritical water gasification of glucose in fluidized bed reactor: A numerical study. *Int. J. Hydrogen Energy* **2017**, *42*, 7857–7865. [CrossRef]
24. Adnan, M.; Sun, J.; Ahmad, N.; Wei, J.J. Comparative CFD modeling of a bubbling bed using a Eulerian–Eulerian two-fluid model (TFM) and a Eulerian-Lagrangian dense discrete phase model (DDPM). *Powder Technol.* **2021**, *383*, 418–442. [CrossRef]
25. Ding, J.; Gidaspow, D. A bubbling fluidization model using kinetic theory of granular flow. *Aiche J.* **2010**, *36*, 523–538. [CrossRef]